A Large-scale Shock Surrounding a Powerful Radio Galaxy?

Croston, J. H.; Hardcastle, M. J.; Mingo, B.; Evans, D. A.; Dicken, D.; Morganti, R.; Tadhunter, C. N.

Published in:
Astrophysical Journal Letters

DOI:
10.1088/2041-8205/734/2/L28

Publication date:
2011

The Astrophysical Journal Letters, 734:L28 (5pp), 2011 June 20 doi:10.1088/2041-8205/734/2/L28

A LARGE-SCALE SHOCK SURROUNDING A POWERFUL RADIO GALAXY?

J. H. Croston[1], M. J. Hardcastle[2], B. Mingo[2], D. A. Evans[3,4], D. Dicken[5], R. Morganti[6,7], and C. N. Tadhunter[8]
[1] School of Physics and Astronomy, University of Southampton, Southampton, SO17 1BJ, UK; J.Croston@soton.ac.uk
[2] School of Physics, Astronomy and Mathematics, University of Hertfordshire, Hatfield, Hertfordshire, AL10 9AB, UK
[3] Harvard-Smithsonian Center for Astrophysics, 60 Garden Street, Cambridge, MA 02138, USA
[4] Department of Physics, Elon University, 2625 Campus Box, Elon, NC 27244, USA
[5] Department of Physics and Astronomy, Rochester Institute of Technology, 84 Lomb Memorial Drive, Rochester, NY 14623, USA
[6] Netherlands Institute for Radio Astronomy, Postbus 2, 7990 AA, Dwingeloo, The Netherlands
[7] Kapteyn Astronomical Institute, University of Groningen, P.O. Box 800, 9700 AV Groningen, The Netherlands
[8] Department of Physics and Astronomy, University of Sheffield, Sheffield S3 7RH, UK
Received 2010 November 26; accepted 2011 May 10; published 2011 May 26

ABSTRACT

We report *Chandra* evidence for a 200 kpc scale shock in the cluster surrounding the powerful radio galaxy 3C 444. Our 20 ks observation allows us to identify a clear surface brightness drop around the outer edge of the radio galaxy, which is likely to correspond to a spheroidal shock propagating into the intracluster medium. We measure a temperature jump across this drop of a factor $\sim$1.7, which corresponds to a Mach number of $\sim$1.7. This is likely to be an underestimate due to the need to average over fairly large regions. We also detect clear cavities corresponding to the positions of the radio lobes, which is only the second such detection associated with an FRII radio galaxy. We estimate that the total energy transferred to the environment is $>8.2 \times 10^{60}$ erg, corresponding to a jet power $>2.9 \times 10^{45}$ erg s^{-1}. Our results suggest that energy input from FRII radio galaxies is likely to exceed substantially estimates based on cluster cavity scaling relations.

Key words: galaxies: active – galaxies: jets

1. INTRODUCTION

The presence of large-scale shocks surrounding powerful radio galaxies has long been a prediction from models of their evolution (e.g., Scheuer 1974; Kaiser & Alexander 1997), and it was realized prior to the launch of the *Chandra X-ray Observatory* that such shocks in radio-galaxy environments should be detectable with our current generation of X-ray instruments (e.g., Heinz et al. 1998). Deep *Chandra* observations have now firmly identified weak shocks in the intracluster medium (ICM) surrounding nearby low-power (FRI: Fanaroff & Riley 1974 class 1) sources, such as Perseus, Hydra A, and M87 (e.g., Fabian et al. 2003; Nulsen et al. 2005b; Forman et al. 2007), and a few examples of strong shocks have been found surrounding smaller sources (e.g., Kraft et al. 2003; Croston et al. 2007; Croston et al. 2009).

Recent work investigating radio-galaxy impact with large samples (e.g., Dunn & Fabian 2008; Bîrzan et al. 2008; Cavagnolo et al. 2010) has also tended to focus on lower power objects, for two major reasons. First, their role as a means of feedback in galaxy evolution is currently perceived to be more important due to their higher number density and ubiquity at the centers of "cool-core" clusters (e.g., Cavagnolo et al. 2008). In addition, most X-ray cavity and weak shock detections to date are associated with FRI radio galaxies, due mainly to the relative scarcity of FRIIs in the nearby clusters where cavities and shocks can easily be detected, but also perhaps partly due to the presence of X-ray inverse-Compton emission which dominates over thermal emission from the ICM for many nearby FRII radio galaxies in poorer environments (e.g., Croston et al. 2005; Kataoka & Stawarz 2005).

Shocks surrounding powerful FRII radio galaxies have so far proved somewhat elusive, although there is evidence for a large-scale shock surrounding Cygnus A (Smith et al. 2002) and a weak shock surrounding the intermediate FRI/II radio-galaxy Hercules A (Nulsen et al. 2005a). The investigation of shocks around FRII radio galaxies is important, however, as they could play a role in galaxy feedback at high redshift (e.g., Rawlings & Jarvis 2004). Detections of shocks and cavities associated with FRII radio galaxies offer an independent means of investigating the conclusions of inverse-Compton and environmental studies, which suggest that FRII radio galaxies are typically close to equipartition between radiating particles and magnetic field, and do not require a significant proton population for pressure balance (e.g., Croston et al. 2005; Kataoka & Stawarz 2005), in contrast to the FRI population (e.g., Croston et al. 2008a). A few FRIIs in rich cluster environments appear to deviate from this conclusion (e.g., Belsole et al. 2007; Hardcastle & Croston 2010), which might indicate a relationship between particle content and environment. It is important to establish whether such a relationship exists in order to account correctly for the energetics of different radio-galaxy populations within galaxy feedback models.

Here we report evidence for a large-scale shock surrounding the weak-lined FRII radio galaxy 3C 444 ($z = 0.153$, $L_{1.4\,\mathrm{GHz}} = 3.3 \times 10^{26}$ W Hz^{-1}), which is found at the center of the cluster A3847 ($L_X \sim 10^{44}$ erg s^{-1}—see below), and present an investigation of its dynamics and energetics. Throughout the Letter we use a cosmology in which $H_0 = 70$ km s^{-1} Mpc^{-1}, $\Omega_\mathrm{m} = 0.3$, and $\Omega_\Lambda = 0.7$, corresponding to an angular scale of 2.66 kpc arcsec^{-1} at this redshift. Galactic absorption of $N_\mathrm{H} = 2.51 \times 10^{20}$ cm^{-2} is assumed for all X-ray spectral fits. Spectral indices α are defined in the sense $S_\nu \propto \nu^{-\alpha}$. Reported errors are 1σ for one interesting parameter, except where otherwise noted.

2. OBSERVATIONS AND DATA ANALYSIS

We observed 3C 444 with the *Chandra* ACIS-S detector for 20 ks on 2009 March 20, as part of a program to complete observations of the southern 2 Jy sample of radio galaxies (Tadhunter et al. 1993; Morganti et al. 1993). The observation

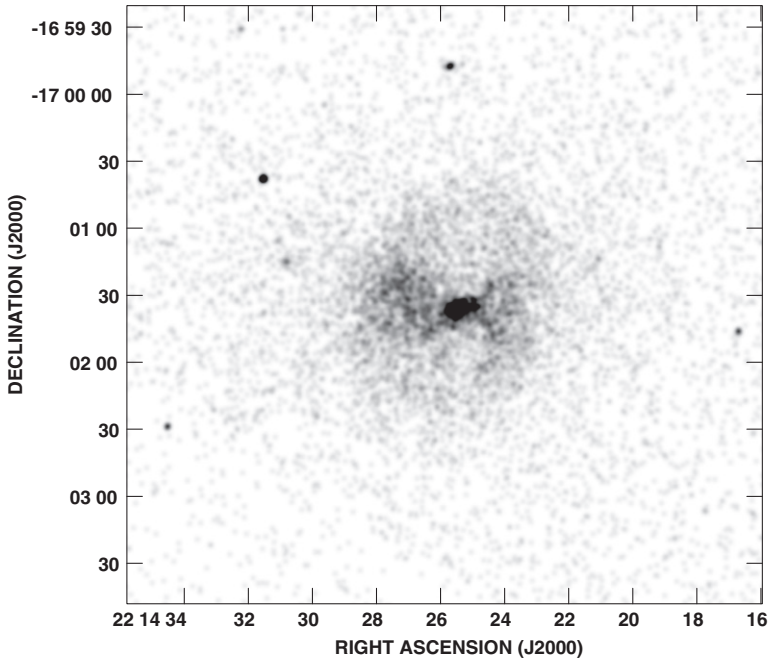

Figure 1. 0.5–5.0 keV image of the *Chandra* data, lightly smoothed with a Gaussian kernel of $\sigma = 3$ pixels.

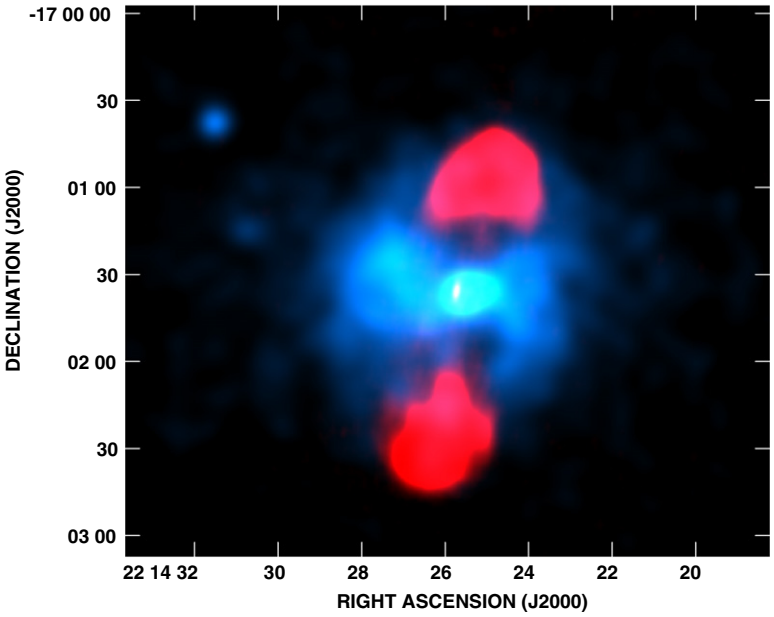

Figure 2. Image made from the *Chandra* data (shown in blue, smoothed with a Gaussian of $\sigma = 15$ pixels) and the 5 GHz VLA map (shown in red), indicating the relationship between the radio and X-ray structures, including cavities at the position of the radio lobes, and a sharp elliptical surface brightness drop surrounding the source.

was taken in VFAINT mode to minimize the background level. The data were reprocessed from the level 1 events file with CIAO 4.2 and CALDB 4.3, including VFAINT cleaning. The latest gain files were applied and the 0.5 pixel randomization was removed using standard techniques.[9] An inspection of the light curve for our observation using the *analyze_ltcrv* script showed no periods of high background level, and so no additional good-time-interval filtering was applied. The radio analysis in this Letter is based on archival Very Large Array (VLA) observations at 1.4 GHz and 5 GHz (program ID AD276). The data were calibrated and imaged within AIPS in the standard manner.

We produced a 0.5–5 keV filtered image from the *Chandra* data to examine the X-ray emission associated with the radio galaxy and environment, which is presented in Figure 1. The relationship between the X-ray and radio emission is shown in Figure 2. Extended emission associated with the surrounding galaxy cluster is clearly detected, with prominent cavities at the positions of the two radio lobes. This is only the second detection of clear cavities associated with a radio galaxy that can be unambiguously classified as an FRII based on its morphology (narrow collimated jets and a compact hot spot in the northern lobe) and radio luminosity. The X-ray surface brightness also decreases noticeably beyond an elliptical region enclosing the radio galaxy.

[9] http://asc.harvard.edu/ciao/

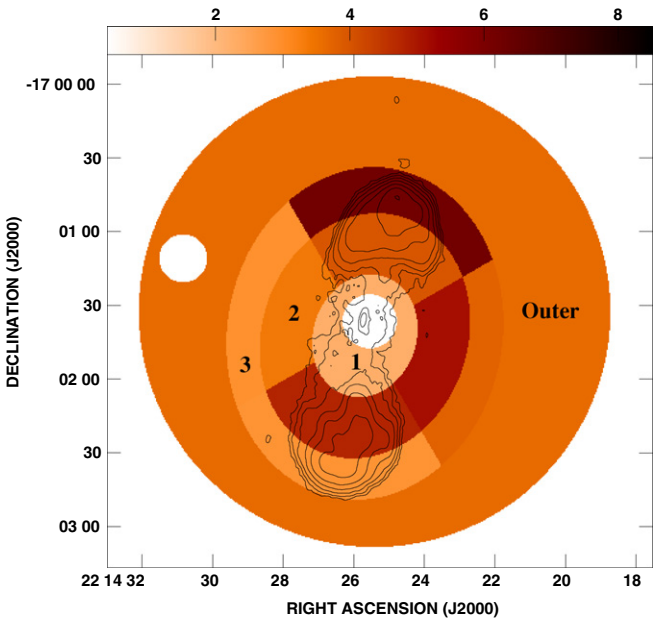

Figure 3. Temperature map (in keV) produced using the results of the spectral fits in Table 1 (regions as in Figure 1), with 5 GHz contours overlaid. White regions do not have measured temperatures. The small circle to the east is a contaminating point source excluded from the fits. The regions used in Table 1 are indicated with annulus numbers/region names.

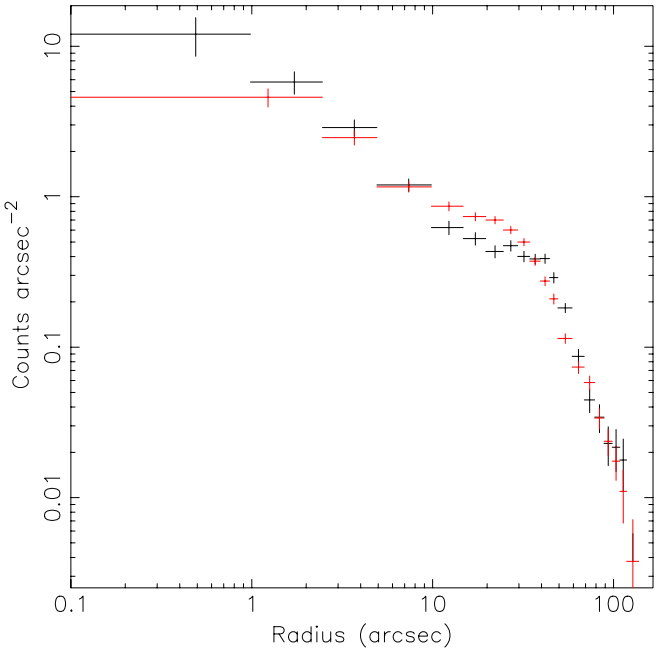

Figure 4. X-ray surface brightness profiles of the emission surrounding 3C 444. The emission was divided into four quadrants, with the north and south quadrants combined to make a longitudinal profile (black) and the east and west quadrants combined to make a transverse profile (red). A sharp drop is present in the N–S direction at ∼45 arcsec, while a less sharp drop is present at ∼30 arcsec in the E–W direction.

We extracted a global spectrum for the cluster (using a circular region of radius 100″, excluding the central 2″ and the radio lobes to avoid non-thermal contamination) and fitted an APEC[10] model to characterize its global properties. We obtain a good fit with a single-temperature model ($\chi^2 = 114$ for 141 dof) with $kT = 3.5 \pm 0.2$ keV, and a bolometric X-ray luminosity of 1.0×10^{44} erg s^{-1}, consistent with a moderately rich cluster and in line with observed L_X–T_X relations (e.g., Pratt et al. 2009). The overall X-ray morphology is very regular, apart from the X-ray cavities, and as reported later (Table 1 and Figure 4) we observe a moderate decrease in central temperature and peak in surface brightness. We classify the cluster as a borderline cool-core cluster using the classification of Pratt et al. (2009), which is based on comparison with a threshold in central density obtained from extrapolation of the surface brightness profile within $0.03R_{500}$.

In order to investigate whether the observed surface brightness decrease is associated with a shock, we extracted surface brightness profiles and spectra in several regions of interest, indicated in Figure 3. Figure 4 shows the surface brightness profiles in the north–south (N–S) and east–west (E–W) directions. In both directions the profile flattens in a way not typically seen in undisturbed cluster profiles (e.g., Cavagnolo et al. 2009) and then drops steeply. The steepening is sharpest in the N–S direction, where there is an abrupt turnover at a distance of ∼45 arcsec.

Spectra for eight annular quadrants as well as the inner and outer regions were fitted with the APEC model (see Table 1). The abundance was poorly constrained in free abundance fits, and so we report the results of fits with abundance fixed at 0.3× solar abundance (using the scale of Anders & Grevasse 1989). A crude temperature map using the same regions is shown in Figure 3. Spectral results for the active galactic nucleus will be presented in B. Mingo et al. (2011, in preparation). The nuclear count rate is insignificant compared to the emission from the cluster gas, and so is not a contaminating source of non-thermal emission for our analysis.

Table 1
Results of Spectral Modeling for Cluster Gas Emission and Radio Lobes[a]

Region	Subregion/Model	Temperature (keV)	Γ	χ^2	dof
Annulus 1		2.2 ± 0.2		36.5	39
Annulus 2	N	$4.0^{+0.7}_{-0.6}$		24.6	27
	E	$3.4^{+0.4}_{-0.3}$		28.8	39
	S	$4.8^{+1.1}_{-0.8}$		10.2	19
	W	$5.1^{1.1}_{-0.8}$		31.4	28
Annulus 3	N	$6.2^{+2.2}_{-1.3}$		11.3	19
	E	$2.9^{+0.6}_{-0.5}$		8.3	14
	S	$2.9^{+1.1}_{-0.6}$		1.2	6
	W	$3.8^{+1.6}_{-1.0}$		4.5	7
Outer region		$3.6^{+0.5}_{-0.4}$		58.8	62
Lobes	PL		1.78 ± 0.04	82.5	71
	APEC	3.91 ± 0.33		63.8	71
	PL + APEC[b]	3.7 ± 0.5	1.7[c]	63.7	70

Notes.
[a] All spectral fits are in the energy range 0.4–7 keV, using an APEC model with abundance fixed at 0.3× solar abundance, using the scale of Anders & Grevasse 1989.
[b] The 0.4–7.0 keV unabsorbed flux was measured to be $<3.1 \times 10^{13}$ erg cm^{-2} s^{-1} and $(5.2^{+0.7}_{-1.8}) \times 10^{-13}$ erg cm^{-2} s^{-1} for the PL and APEC components, respectively.
[c] The power-law photon index tended to very low values of ∼0.3, and so we fixed its value at a physically reasonable value for lobe inverse-Compton emission so as to test the possible presence of such a component.

The results of spectral fitting to the radio lobe regions (extraction regions chosen to encompass the extent of radio emission) are listed in Table 1. The detection of X-ray cavities in our *Chandra* data indicates that lobe inverse-Compton

[10] Astrophysical Plasmas Emission Code: http://www.atomdb.org.

emission (cf. Croston et al. 2005) is weak relative to the cluster X-ray emission; however, it is important to be certain that non-thermal emission cannot contaminate our spectral results. A thermal model was a significantly better fit than a power-law model to the lobe regions (Table 1); however, a thermal + power-law model also gave a good fit with a significant power-law contribution, corresponding to a 1 keV flux density of 9 nJy, which is a factor of ∼4 higher than the inverse compton (IC) prediction at equipartition (based on modeling using the code of Hardcastle et al. 1998). Such a departure from equipartition is consistent with the results for the FRII population (e.g., Croston et al. 2005); however, the presence of this component is not required by the data. Reassuringly, the temperature of the thermal component in the model is not significantly affected by the presence of a power-law contribution at this level. IC emission at a higher level is unlikely: our previous work on large samples of FRII radio galaxies has shown that the level of lobe IC is narrowly distributed, with a mean level a factor 2–3 above the equipartition prediction. We therefore conclude that our temperature measurements are not affected by inverse-Compton contamination.

3. EVIDENCE FOR A SHOCK SURROUNDING 3C 444

As shown in Figure 4, the surface brightness in the N–S direction drops steeply by a factor of ∼10 between 45 and 70 arcsec from the cluster center. It is difficult to robustly estimate the position of this jump from the (circularly symmetric) profile, as its location in the north and south appears different—the effective radius is underestimated because of averaging over the two quadrants and to the sides of the radio source where the elliptical shock front would be expected to be closer to the center. The abrupt transition from a flat profile between 15″ and 45″ to a steep drop to ∼70″ cannot be fitted by standard galaxy-cluster profile models such as a beta model, and so is likely to be caused by the influence of the expanding radio lobes. The surface brightness decrease corresponds roughly to a density jump of a factor of ∼3, consistent with the presence of a moderately strong expanding shock wave surrounding the radio lobes of 3C 444 at a distance of ∼200 kpc from the cluster center. Further evidence for the presence of a shock comes from our spectral analysis: there is a temperature jump of a factor 1.7 ± 0.4 at the edge of the north lobe, based on comparing the temperature in the northern quadrant of Annulus 3 (Table 1) with an outer region encompassing all radii. A more robust conclusion could be made using an outer temperature measurement for the northern quadrant only; however, a spectral fit to this region, while giving a temperature measurement consistent with that of the larger "outer region" used, is too poorly constrained to provide conclusive evidence of a temperature jump. This temperature jump corresponds to a Mach number of 1.7 ± 0.4, suggesting that a shock is indeed present. The Mach number calculated is significantly lower than that implied by the surface brightness jump, $\mathcal{M} \sim 3$. This may be because the temperature jump is underestimated due to averaging the hottest emission regions with cooler material further from the shock, or could be partly due to the geometrical and uniform density assumptions. The temperature structure around the south radio lobe is difficult to interpret in the context of this shock scenario, as the temperature appears highest in a region in the middle of the lobe and comparatively cool (∼3 keV) at the outer edge. The reason for this is unclear—projection effects could mean that the lobe is expanding fastest in the direction toward the line of sight, or asymmetries in the ICM density of temperature distribution could lead to slower expansion of the southern lobe. Neither of these explanations is entirely satisfactory, but the shock interpretation remains most plausible for the northern temperature structure; deeper X-ray data are required to obtain a clearer understanding of the relationship between temperature structure and radio-lobe behavior.

4. DYNAMICS AND ENERGETIC IMPACT OF 3C 444

To investigate further the source dynamics and energetic impact, we estimated the external pressure surrounding the outer radio lobes and compared it with the internal radio lobe pressure under various assumptions. We estimated the external pressure acting on the radio lobes by considering the northern and southern quadrants of Annuli 2 and 3. We assumed each region had the geometry of an ellipsoidal shell (subtracting the overlapping volume of the radio lobe in each case) with a constant density and a temperature corresponding to the mean of the two spectral regions in each direction (Table 1). We determined densities of $n_{\rm p} = 0.0047$ and 0.0036 cm^{-3} for the northern and southern quadrants, respectively, which correspond to external pressures of $\sim 8.4 \times 10^{-12}$ Pa and $\sim 4.9 \times 10^{-12}$ Pa, respectively. Taking into account geometrical uncertainties in estimating the densities, and uncertainties on the temperature measurements, the pressure uncertainties are at most ∼40%. The internal lobe pressures were determined under the assumption of no protons in three different scenarios: (1) equipartition between magnetic field and radiating particles; (2) a magnetic field strength $B = 0.7 B_{\rm eq}$, the median found for FRII radio galaxies in the inverse-Compton study of Croston et al. (2005); and (3) the magnetic field strength leading to inverse-Compton emission just below the measured upper limit for the lobes of 9 nJy at 1 keV (see Section 2 above). These gave pressures for the north lobe of 3.6×10^{-13} Pa (scenario 1), 9×10^{-13} Pa (scenario 2), and 2.1×10^{-12} Pa (scenario 3), and for the south lobe of 2.3×10^{-13} Pa (scenario 1), 6.7×10^{-13} Pa (scenario 2), and 1.3×10^{-12} Pa (scenario 3). A comparison with the external pressure measured above ($P_{\rm ext}/P_{\rm int} \sim$ 14–23, 5–9, and 4–6, respectively, for the three scenarios above) demonstrates that the lobes would be underpressured in all of these scenarios, indicating that non-radiating particles (e.g., protons) are likely to dominate the lobe pressure. An apparent pressure imbalance of this sort is commonly found for low-power radio galaxies (e.g., Croston et al. 2008), but the good agreement with equipartition magnetic fields from inverse-Compton studies has previously been used to argue against a significant proton population in FRII radio galaxies (e.g., Croston et al. 2005). Environmental pressure comparisons for powerful FRII radio galaxies (e.g., Croston et al. 2004; Belsole et al. 2007) indicate that in general the requirements for proton content are smaller than in FRI radio galaxies; however, FRII radio galaxies in the most rich environments appear more proton-dominated (Belsole et al. 2007; Hardcastle & Croston 2010). This supports the argument of Croston et al. (2008) that radio-galaxy particle content on large scales is related to radio morphology, which may indicate the radio jets' ability to entrain material from the surroundings.

The thermal proton density in the heated region immediately surrounding the northern lobe edge was also used to estimate the total energetic impact of the radio galaxy. Assuming that the material in this region has been heated from the measured pre-shock temperature of 3.6 keV, the total "excess" energy in the hot region is $\sim 8.2 \times 10^{60}$ erg. If the lobes are assumed slightly overpressured (e.g., $\sim 1.5 \times P_{\rm ext}$), consistent with the observed shock, then the work done by the northern lobe is $1.5 P_{\rm ext} V \sim 1.4 \times 10^{60}$ erg, a factor of ∼6 lower than the required

heating. Note that as we have ignored any heating in the E, W, and S quadrants, the measured energy input could therefore be considered a lower limit.

We estimated the lobe inflation timescale by considering the inflation time if the expansion was constant at the currently observed shock speed of $\mathcal{M} \sim 1.7$. This is likely to be an upper limit since the radio source would be expected to undergo a phase of faster expansion at early times. The $\mathcal{M} = 1.7$ timescale is 9×10^7 years, implying a jet power of $P_{\rm jet} = 2.9 \times 10^{45}$ erg s^{-1}. We also determined a radio spectral age for the lobes by fitting a standard Jaffe & Perola (1973) model to the steep-spectrum emission from the inner part of the radio lobes, as measured from matched resolution 1.4 and 5 GHz radio maps, assuming a low-frequency spectral index at the hot spots of $\alpha = 0.5$. We used the two estimates of the magnetic field strength discussed in Section 3. Spectral ages of 2.3×10^7 years and 4.6×10^7 years were obtained for the assumptions of an equipartition field (1.05 nT) and of the B field required for our X-ray IC upper limit (0.5 nT), respectively. The true magnetic field is expected to lie between these values. Jet powers using our two spectral age timescales are 10^{46} and 6×10^{45} erg s^{-1}, for the equipartition and IC B field assumptions, respectively. The 1.4 GHz radio luminosity of 3C 444 is $L_{1.4\,\rm GHz} = 3.3 \times 10^{26}$ W Hz^{-1}, and so our estimated mechanical power is somewhat high for the source luminosity, compared with the relation of Bîrzan et al. (2008), but within the observed scatter. As far as we are aware, this is only the second jet power estimate from X-ray environmental observations, after Cygnus A, for a radio galaxy that can be classed unambiguously as an FRII based on both radio morphology and luminosity. Our result for 3C 444 suggests that using an average relation from cluster cavity results (e.g., Bîrzan et al. 2008) is likely to underestimate the mechanical output of FRII radio galaxies. This result is therefore important for constraining the poorly known high-luminosity end of the relation between jet power and radio luminosity.

5. CONCLUSIONS

We have identified a likely 200 kpc scale shock in the cluster environment of the radio galaxy 3C 444, based on a sharp surface brightness drop-off and significant temperature increases at the edges of the radio lobes. We infer that the radio galaxy has injected a total energy ~8 times the work done by the radio lobes assuming pressure balance, which implies that estimates of FRII radio galaxy energy input based simply on PdV work will be underestimates due to the role of shock heating. We estimate a total energy input from the expanding radio galaxy of 8.2×10^{60} erg, which implies a jet power of $(0.3–1.0) \times 10^{46}$ erg s^{-1}. Finally, based on a comparison of the external pressure with the internal pressure, we conclude that a significant proton contribution to the internal pressure is required, which is unexpected for an FRII galaxy given the good agreement of inverse-Compton measurements with the minimum energy condition for the population as a whole. However, this is consistent with results for a handful of other powerful radio galaxies in rich environments and suggests a strong role for environmental interactions in determining particle and energy content.

J.H.C. acknowledges support from the South-East Physics Network (SEPnet). M.J.H. thanks the Royal Society for support via a University Research Fellowship. We thank the anonymous referee for useful comments that have enabled us to improve the Letter.

REFERENCES

Anders, E., & Grevesse, N. 1989, Geochim. Cosmochim. Acta, 53, 197
Belsole, E., Worrall, D. M., Hardcastle, M. J., & Croston, J. H. 2007, MNRAS, 381, 1109
Bîrzan, L., McNamara, B. R., Nulsen, P. E. J., Carilli, C. L., & Wise, M. W. 2008, ApJ, 686, 859
Cavagnolo, K. W., Donahue, M., Voit, G. M., & Sun, M. 2008, ApJ, 683, 107
Cavagnolo, K. W., Donahue, M., Voit, G. M., & Sun, M. 2009, ApJS, 182, 12
Cavagnolo, K. W., McNamara, B. R., Nulsen, P. E. J., Carilli, C. L., Jones, C., & Bîrzan, L. 2010, ApJ, 720, 1066
Croston, J. H., Birkinshaw, M., Hardcastle, M. J., & Worrall, D. M. 2004, MNRAS, 353, 879
Croston, J. H., Hardcastle, M. J., Birkinshaw, M., Worrall, D. M., & Laing, R. A. 2008, MNRAS, 386, 1709
Croston, J. H., Hardcastle, M. J., Harris, D. E., Belsole, E., Birkinshaw, M., & Worrall, D. M. 2005, ApJ, 626, 733
Croston, J. H., Kraft, R. P., & Hardcastle, M. J. 2007, ApJ, 660, 191
Croston, J. H., et al. 2009, MNRAS, 395, 1999
Dunn, R. J. H., & Fabian, A. C. 2008, MNRAS, 385, 757
Fabian, A. C., Sanders, J. S., Allen, S. W., Crawford, C. S., Iwasawa, K., Johnstone, R. M., Schmidt, R. W., & Taylor, G. B. 2003, MNRAS, 344, 43
Fanaroff, B. L., & Riley, J. M. 1974, MNRAS, 167, 31
Forman, W. R., et al. 2007, ApJ, 665, 1057
Hardcastle, M. J., Birkinshaw, M., & Worrall, D. M. 1998, MNRAS, 294, 615
Hardcastle, M. J., & Croston, J. H. 2010, MNRAS, 404, 2018
Heinz, S., Reynolds, C. S., & Begelman, M. C. 1998, ApJ, 501, 126
Jaffe, W. J., & Perola, G. C. 1973, A&A, 26, 423
Kaiser, C. R., & Alexander, P. 1997, MNRAS, 286, 215
Kataoka, J., & Stawarz, L. 2005, ApJ, 622, 797
Kraft, R. P., Vazquez, S. E., Forman, W. R., Jones, C., Murray, S. S., Hardcastle, M. J., Worrall, D. M., & Churazov, E. 2003, ApJ, 592, 129
Morganti, R., Killeen, N. E. B., & Tadhunter, C. N. 1993, MNRAS, 263, 1023
Nulsen, P. E. J., Hambrick, D. C., McNamara, B. R., Rafferty, D., Bîrzan, L., Wise, M. W., & David, L. P. 2005a, ApJ, 625, 9
Nulsen, P. E. J., McNamara, B. R., Wise, M. W., & David, L. P. 2005b, ApJ, 628, 629
Pratt, G. W., Croston, J. H., Arnaud, M., & Böhringer, H. 2009, A&A, 498, 361
Rawlings, S., & Jarvis, M. J. 2004, MNRAS, 355, 9
Scheuer, P. A. G. 1974, MNRAS, 166, 513
Smith, D. A., Wilson, A. S., Arnaud, K. A., Terashima, Y., & Young, A. J. 2002, ApJ, 565, 195
Tadhunter, C. N., Morganti, R., di Serego-Alighieri, S., Fosbury, R. A. E., & Danziger, I. J. 1993, MNRAS, 263, 999